

Interferometric hydrofracture microseism localization using neighboring fracture

Oleg V. Poliannikov¹, Alison E. Malcolm¹, Hugues Dijkpesse², and Michael Prange²

ABSTRACT

Hydraulic fracturing is the process of injecting high-pressure fluids into a reservoir to induce fractures and thus improve reservoir productivity. Microseismic event localization is used to locate created fractures. Traditionally, events are localized individually. Available information about events already localized is not used to help estimate other source locations. Traditional localization methods yield an uncertainty that is inversely proportional to the square root of the number of receivers. However, in applications where multiple fractures are created, multiple sources in a reference fracture may provide redundant information about unknown events in subsequent fractures that can boost the signal-to-noise ratio, improving estimates of the event positions. We used sources in fractures closer to the monitoring well to help localize events further away. It is known through seismic interferometry that with a 2D array of receivers, the traveltimes between two sources may be recovered from a

crosscorrelogram of two common source gathers. This allowed an event in the second fracture to be localized relative to an event in the reference fracture. A difficulty became evident when receivers are located in a single monitoring well. When the receiver array is 1D, classical interferometry cannot be directly employed because the problem becomes underdetermined. In our approach, interferometry was used to partially redatum microseismic events from the second fracture onto the reference fracture so that they can be used as virtual receivers, providing additional information complementary to that provided by the physical receivers. Our error analysis showed that, in addition to the gain obtained by having multiple physical receivers, the location uncertainty is inversely proportional to the square root of the number of sources in the reference fracture. Because the number of microseism sources is usually high, the proposed method will usually result in more accurate location estimates as compared with the traditional methods.

INTRODUCTION

Hydraulic fracturing enhances the production of hydrocarbons and other fluids from rock formations. It is a critical tool in many applications, including shale gas and geothermal energy production. The process of hydraulic fracturing involves injecting fluids under high pressure into a reservoir formation with the purpose of creating additional fluid pathways leading to the production well. These pathways may have complicated shapes; however, fractures aligned with the direction of maximum stress are commonly observed (Zoback et al., 2003). Knowing where hydraulic fractures have been created helps in predicting fluid flow, designing additional fractures, and positioning additional production wells.

Hydraulic fracture creation is normally accompanied by microseismic events (microseisms) thought to be generated by the cracking of the rock. Locating these microseisms is an indirect method of fracture imaging and fracture growth monitoring in near real time. To locate these microseisms, an array of three-component receivers is often installed in one or several monitoring wells. Arrivals from each microseismic event are recorded for each receiver. These recordings are then used to locate the microseisms. The problem of localizing events from this type of data has received considerable attention (Michaud et al., 2004; Huang et al., 2006; Bennett et al., 2006). Despite significant progress, the problem remains a challenge in need of further investigation due to large localization uncertainties.

Manuscript received by the Editor 6 October 2010; revised manuscript received 17 February 2011; published online 30 December 2011; corrected version published online 18 January 2012.

¹Massachusetts Institute of Technology, Department of Earth, Atmospheric and Planetary Sciences, Earth Resources Laboratory, Cambridge, Massachusetts, USA. E-mail: poliann@mit.edu; amalcolm@mit.edu.

²Schlumberger-Doll Research, Cambridge, Massachusetts, USA. E-mail: HDijkpesse@slb.com; prange@slb.com.
© 2011 Society of Exploration Geophysicists. All rights reserved.

Most techniques currently employed by the industry locate events one by one. The estimate of the location of one event is not used to improve the estimate of another. For microseism localization from a single observation well, the traveltime from each microseism to the receiver is picked, and the wave's polarization is estimated. The polarization provides the direction of the arriving wave as it impinges on the receiver. The polarization and the traveltime along with an assumed velocity model, allow us to ray trace to the inferred event location. We shall refer to this as the classical localization technique. The event excitation time is not known in practice, but this problem may be eliminated by considering the time difference between P and S arrivals (Pearson, 1981; House, 1987). In our analysis of the classical approach, we will assume for simplicity that the event excitation time is known. This time is not needed for the interferometric method proposed in this paper. The goal of this paper is not to characterize the performance of state-of-the-art proprietary algorithms of the non-interferometric type, but to contrast controlling mechanisms for localization uncertainty in the classical approach with those for our new interferometric approach.

In practice, multiple fractures are created sequentially. One fracture can often be created close to the monitoring well, with other fractures appearing further away, as shown in Figure 1. This geometry dictates that sources corresponding to the closest fracture can be imaged better with traditional methods than those in further fractures because the velocity is likely to be better constrained near the observation well, and the receivers form a larger angular coverage relative to the fracture event locations. Instead of locating events in a more distant fracture independently, we would like to use available information about the reference (closest) fracture to improve the estimated locations in the more distant fractures. We will use seismic interferometry to couple together events from both fractures. Under idealized assumptions, interferometry recovers the Green's function between any two source locations. Those assumptions are rarely satisfied in practice, and for a single borehole, the full recovery of the Green's function between two source locations is fundamentally impossible. The signal recorded in the well can be only partially redatumed to an event in the first fracture. The end result of the redatuming process is not the complete Green's function, but partial information about it. We show in this paper, however, that this information, along with an assumed velocity

model, can significantly reduce uncertainty around the estimated event location as compared to the classical method.

Interferometry provides additional advantages by leading to stable imaging in the presence of velocity uncertainty (Borcea et al., 2005). We will not explore the full range of potential benefits provided by interferometry, but rather, how it can be used to improve microseismic event localization in a canonical case and explain its fundamental limitations.

We propose using interferometry to partially redatum every noisy record of an event from a second fracture onto a reference fracture. Using this approach, in addition to measuring events in the second fracture with physical receivers in the monitoring well, we obtain additional information from the many virtual receivers located in the reference fracture. This redundancy boosts the signal-to-noise ratio (S/N) and reduces the localization uncertainty. For classical methods, a higher S/N is achieved by appropriately stacking over all available receivers. In the method proposed in this paper, additional information coming from events in the reference fracture is also stacked over. Because the number of events in the reference fracture is typically much higher than the number of physical receivers in the observation well, we can expect a considerable improvement over the performance of the classical algorithm. We present the theory and show numerical examples that illustrate this result.

PROBLEM SETUP

Assume that the velocity model is known with sufficient accuracy to compute traveltimes. A monitoring well is instrumented with N_{rec} three-component receivers with locations $x_{\text{rec}} \in \mathcal{W}$, where \mathcal{W} denotes the monitoring well. The signals recorded at the receivers are seismograms that are assumed to contain direct arrivals from each event in each of two fractures. We also assume that the observed seismograms are perturbed by additive uncorrelated Gaussian noise that models measurement errors. Denote the two fractures as \mathcal{F}_1 and \mathcal{F}_2 and assume that \mathcal{F}_1 is closer to the monitoring well than \mathcal{F}_2 . For convenience, we think of the two fractures as being roughly parallel to one another (Figure 1). This is not a necessary assumption, however, and deviations from it are allowed. Indeed, in our usage here, a fracture is merely a collection of source events.

We first assume for simplicity that the events of the reference fracture \mathcal{F}_1 have been located precisely. These microseismic locations are denoted by $x_{s,1} \in \mathcal{F}_1$. In a later section, we will generalize our results to a more realistic situation where the event locations in the first fracture have some uncertainty. Our goal is to localize events $x_{s,2} \in \mathcal{F}_2$.

IMPROVED LOCALIZATION FROM INTERFEROMETRY

In this section, we present the interferometric method of event localization using data recorded from a single monitoring well. We begin by presenting a simplified localization technique, which we use as a benchmark. This is followed by a brief summary of classical interferometry, which inspired our method. When only single well data is available, classical interferometry is no longer fully applicable. However, by performing a stationary phase analysis of 1D correlogram events, we are able to extract partial information about unknown event locations from reference event locations. The proposed method is illustrated using both a homogeneous and layered velocity model.

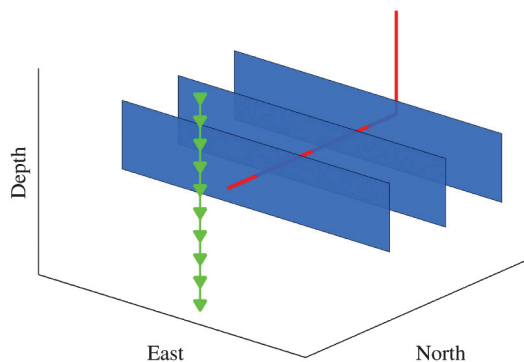


Figure 1. Water is injected under pressure through the treatment well (red line), which creates multiple fractures (blue planes). The process is seismically monitored from the observation well (green). These fractures are shown as planes, but in practice are complex shapes that are localized as clouds of points.

Classical localization

In this paper, we use a simplified version of a classical localization technique as a point of comparison for our proposed interferometric method. We pick the traveltime t_p of the P-wave from the event to the receiver using a crosscorrelation method with a known source wavelet. Then, we estimate the unit polarization vector $\hat{\mathbf{p}}$ of the P-wave using a method based on a singular value decomposition analysis of the arrival of the P-wave (de Franco and Musacchio, 2001). If the velocity model is homogeneous, then the polarization vector is given by

$$\hat{\mathbf{p}} = \frac{x_{\text{rec}} - x_s}{\|x_{\text{rec}} - x_s\|}, \quad (1)$$

where $\|\cdot\|$ denotes the vector length (ℓ_2 norm). The polarization is a unit-length vector pointing from the event location x_s in the direction of the receiver location x_{rec} . Denoting the homogeneous P-velocity by V_p , an estimate of the source location is given by

$$x_s = x_{\text{rec}} - V_p t_p \hat{\mathbf{p}}. \quad (2)$$

For a general velocity model, the source location is found by tracing a ray that leaves the receiver in the $\hat{\mathbf{p}}$ direction and stops at time t_p . This localization method is perfect if the medium is known exactly, and the observed signal contains no noise. Random noise in the seismograms results in localization uncertainty, which can be reduced by stacking over multiple receivers. More detailed analysis of this uncertainty will be presented in the [Uncertainty analysis](#) section.

Seismic interferometry

Seismic interferometry allows physical sources to be redatumed to receiver locations (Rickett and Claerbout, 1996; Derode et al., 2003; Bakulin and Calvert, 2004; Schuster et al., 2004; Wapenaar et al., 2005; Djikpesse et al., 2009). Receivers can likewise be redatumed to source locations according to the principle of reciprocity (Curtis et al., 2009).

Specifically, suppose that two sources located at $x_{s,1}$ and $x_{s,2}$ inside a 3D medium are surrounded by a closed 2D surface of receivers in the set \mathcal{W} . Although the theory we are developing works in the elastic case, we pick the P- and S-wave traveltimes separately, essentially using acoustic theory for both arrivals. Following Wapenaar (2004), Wapenaar et al. (2005) and Schuster and Zhou (2006), the interferometrically derived Green's function between two source locations may be recovered from the representation theorem, and has the form

$$G(x_{s,2}, x_{s,1}, \omega) + G^*(x_{s,1}, x_{s,2}, \omega) \\ \propto \iint_{x_{\text{rec}} \in \mathcal{W}} G^*(x_{s,1}, x_{\text{rec}}, \omega) G(x_{s,2}, x_{\text{rec}}, \omega) dS, \quad (3)$$

where $G(x_{s,2}, x_{s,1}, \omega)$ is the Green's function between the locations $x_{s,1}$ and $x_{s,2}$ written in the Fourier domain, and the star (*) denotes the complex conjugate. While interferometry may generally be used to redatum entire waveforms, in this work, we are only interested in recovering traveltimes. In particular, we ignore the issue of the source mechanisms of the microseismic events. Note that in this context, even when the surface \mathcal{W} does not completely enclose

the medium, traveltimes along certain rays may be recovered. Specifically, traveltimes may be recovered along rays that are emitted by one source, pass through the other, and are finally received at some receiver location, as shown in Figure 2 (Lu et al., 2008). Mathematically, the traveltime between the sources will come from a stationary phase point in the crosscorrelogram of two common source gathers (Snieder, 2004). The crosscorrelation lag of two direct arrivals from two different sources is a function, $\tau(x_{\text{rec}})$, of the receiver position x_{rec} that belongs to the 2D surface \mathcal{W} . The stationary phase point $(x_{\text{rec}}^0, \tau(x_{\text{rec}}^0))$ is defined by the extremum of the function τ . The stationary receiver location x_{rec}^0 marks the receiver that records the ray connecting the two sources. The stationary value, $\tau(x_{\text{rec}}^0)$, has the physical meaning of the traveltime between the two sources along that ray.

In classical interferometry, receivers enclosing the two sources must span a 2D surface \mathcal{W} . The stationary phase point is found by setting the two partial derivatives of τ in orthogonal directions to zero. Because only one partial derivative can be estimated with a 1D receiver array, the stationary phase condition becomes underdetermined (Figure 2). Stationary points along a 1D receiver array, i.e., single monitoring well, are thus not stationary in the classical sense, but they still give useful information for source localization.

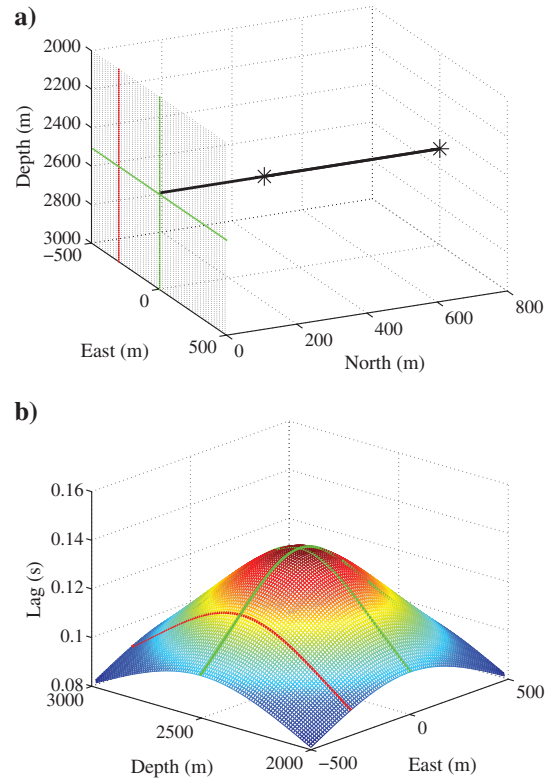


Figure 2. (a) The ray that connects two sources is received at a stationary receiver location within a 2D receiver-array aperture (the intersection of the two green lines). (b) The stationary receiver location is the stationary point of the 2D correlogram. The stationary point is shown as the intersection of two common source gather lags plotted as green curves. A correlogram calculated over a 1D receiver array (red line) may exhibit an extremum, but it need not correspond to any physical ray or yield a physical traveltime.

Interferometric localization using a single monitoring well

The method that we introduce here is applicable to a general velocity model and an arbitrary well geometry subject only to minor technical assumptions. Specifically suppose that receivers are given by their locations:

$$x_{\text{rec}}(\ell) \equiv (x_{\text{rec}}(\ell), y_{\text{rec}}(\ell), z_{\text{rec}}(\ell)), \quad (4)$$

where ℓ is the well arc length measured from the top of the well. Suppose further that we are given a velocity model, from which we compute the traveltime function, $T(x_s, \ell) \equiv T(x_s, x_{\text{rec}}(\ell))$. In what follows, ℓ is a continuous parameter, but in practice, a receiver array consists of a finite number of receivers. We use spline interpolation to obtain traveltimes at locations between physical receivers.

Let $x_{s,1}$ be an event with a known location in the reference fracture. By jointly analyzing the signal emitted from that known location with another signal coming from an event in the second fracture whose location is unknown, we would like to recover at least partial information about the location $x_{s,2}$ of that second fracture.

The correlogram of the direct arrivals from the two events contains a peak with lag:

$$\tau(x_{s,1}, x_{s,2}, \ell) = T(x_{s,2}, \ell) - T(x_{s,1}, \ell). \quad (5)$$

Assuming this lag has a stationary point, ℓ^0 , with respect to the receiver location, we call this a stationary receiver and denote it by $x_{\text{rec}}^0 \equiv x_{\text{rec}}(\ell^0)$. Hence,

$$\partial_{\ell} \tau(x_{s,1}, x_{s,2}, \ell^0) = \left. \frac{\partial \tau(x_{s,1}, x_{s,2}, \ell)}{\partial \ell} \right|_{\ell=\ell^0} = 0. \quad (6)$$

The stationary lag of the event is consequently

$$\tau^0 \equiv \tau(x_{s,1}, x_{s,2}, \ell^0). \quad (7)$$

Observe that the pair consisting of the stationary receiver location and the stationary lag, which we call a stationary condition, are observed directly from the data. Their values tie together the known location $x_{s,1}$ with the unknown location $x_{s,2}$ in the following way. The locus of all points $x_{s,2}$ giving rise to the same stationary condition, $(x_{\text{rec}}(\ell^0), \tau^0)$, is a subset of 3D space defined by

$$\begin{aligned} \mathcal{R}(x_{s,1}, \ell^0, \tau^0) &= \{x_{s,2} | \partial_{\ell} \tau(x_{s,1}, x_{s,2}, \ell^0) = 0 \\ &\text{and } \tau^0 = \tau(x_{s,1}, x_{s,2}, \ell^0)\}. \end{aligned} \quad (8)$$

Provided that the two constraints defining \mathcal{R} are sufficiently smooth, the set \mathcal{R} will be a 1D curve. This curve can be determined numerically, or in some cases, analytically. Because a point $x_{s,2}$ can travel along the curve \mathcal{R} with no change to the stationary condition, we cannot completely localize it using interferometry. We can, however, constrain two out of three coordinates in a suitable coordinate system, i.e., we can place the source on a particular 1D curve but cannot say where on this curve the event lies.

The stationary condition from equation 8 applied to multiple reference events $x_{s,1}$ produces a corresponding number of curves \mathcal{R} . All of those curves by construction contain the unknown event location $x_{s,2}$. If their intersection consisted of a single point, the event $x_{s,2}$ would be successfully localized. However, in some cases,

including the example below, those curves may intersect along a common stretch, which makes the complete event localization impossible. Instead, the method produces multiple estimates of the same stretch of a 1D curve. Appropriate averaging over these estimates should greatly reduce the uncertainty in the direction perpendicular to the stretch and have little effect on the uncertainty along the stretch.

Example: Localization in homogeneous medium

Our general method outlined in previous sections can be easily applied to a horizontally stratified velocity model, as illustrated in the [Numerical results](#) section. For clarity purposes, we consider here the case of a homogeneous velocity model with a constant P-wave velocity V_p and a vertical monitoring well. As the general theory predicts, interferometry allows us to use known events in a reference fracture to constrain two out of the three location parameters of a microseism in \mathcal{F}_2 , and those parameters have a very clear intuitive meaning in this example.

Consider two event locations, $x_{s,1} = (x_{s,1}, y_{s,1}, z_{s,1})$ and $x_{s,2} = (x_{s,2}, y_{s,2}, z_{s,1})$, and a receiver location, $x_{\text{rec}} = (0, 0, z_{\text{rec}})$. The traveltimes from the sources to the receiver are given by

$$T(x_{s,i}, x_{\text{rec}}) = \frac{\sqrt{x_{s,i}^2 + y_{s,i}^2 + (z_{s,i} - z_{\text{rec}})^2}}{V_p}, \quad i = 1, 2.$$

The crosscorrelogram of the two common event gathers contains an event from the correlations of the two direct waves with the lag

$$\begin{aligned} \tau_{x_{s,1}, x_{s,2}}(z_{\text{rec}}) &= \frac{\sqrt{x_{s,2}^2 + y_{s,2}^2 + (z_{s,2} - z_{\text{rec}})^2}}{V_p} \\ &\quad - \frac{\sqrt{x_{s,1}^2 + y_{s,1}^2 + (z_{s,1} - z_{\text{rec}})^2}}{V_p}. \end{aligned} \quad (9)$$

The receiver located at x_{rec} is stationary in the z -direction for the pair of events $x_{s,1}$ and $x_{s,2}$ if

$$\frac{\partial \tau_{x_{s,1}, x_{s,2}}(z_{\text{rec}})}{\partial z_{\text{rec}}} = 0. \quad (10)$$

Combining equation 9 with equation 10, we arrive at the following formula for the stationary receiver depth:

$$z_{\text{rec}}^0 = \frac{r_{s,2} z_{s,1} - r_{s,1} z_{s,2}}{r_{s,2} - r_{s,1}}, \quad r_{s,2} > r_{s,1}, \quad (11)$$

where $r_{s,i} = \sqrt{x_{s,i}^2 + y_{s,i}^2}$ is the horizontal offset from the receiver line to the event location $x_{s,i}$.

We can interpret equation 11 geometrically as follows. Suppose that the two events and the receiver are in the same vertical plane, and both sources are on the same side of the receiver. We may assume, for example, that they both have zero azimuth: $y_{s,1} = y_{s,2} = 0$, and $x_{s,2} > x_{s,1} > 0$. It then follows from equation 11 that

$$z_{\text{rec}}^0 = \frac{z_{s,2} - z_{s,1}}{x_{s,2} - x_{s,1}} (x - x_{s,1}) + z_{s,1} \Big|_{x=0}, \quad (12)$$

and then from equation 9 that

$$\tau_{x_{s,1}, x_{s,2}}(z_{\text{rec}}^0) = \frac{\sqrt{(x_{s,2} - x_{s,1})^2 + (z_{s,2} - z_{s,1})^2}}{V_P}. \quad (13)$$

The physical interpretation of the stationary receiver location and the stationary lag is identical to that in classical interferometry. The stationary receiver lies on the ray that connects the two event locations $x_{s,1}$ and $x_{s,2}$, and the stationary lag is the physical travel-time of the wave between those two points.

Now, consider sources $x_{s,1}$ and $x_{s,2}$ in general 3D positions. Because the solution in equation 11 depends only on the horizontal offset between the two sources, the two sources located at $x_{s,1}$ and $x_{s,2}$ will produce a stationary point at the receiver location x_{rec} so long as the three points ($x_{s,1}$, $x_{s,2}$, and x_{rec}) can be made collinear by appropriate rotations of both sources about the receiver line (Figure 3a). The curve \mathcal{R} , whose general form is given in equation 8, in this simple example, is a ring lying inside a horizontal plane.

It follows from equation 11 that both sources $x_{s,1}$ and $x_{s,2}$ must have the same dip angle when viewed from the receiver location x_{rec} , and that τ is the traveltime between the circle containing $x_{s,1}$ and the circle containing $x_{s,2}$ (see Figure 3b). Write both event locations in spherical coordinates centered at the receiver x_{rec} :

$$x_{s,i} = x_{\text{rec}} + R_i(\cos \theta_i \cos \phi_i, \cos \theta_i \sin \phi_i, \sin \theta_i), \quad i = 1, 2, \quad (14)$$

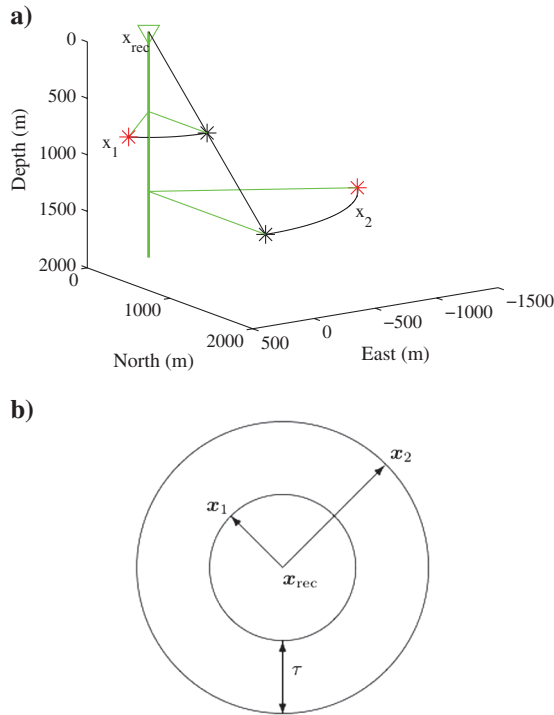


Figure 3. (a) The receiver in a 1D array is vertically stationary with respect to two given sources (red stars) if the source locations can be rotated about the receiver line into collinear positions (black stars). (b) All pairs of sources such that each source belongs to a corresponding circle (shown in a map view) produce a correlogram with identical stationary receiver location and with the same stationary lag.

where θ_i is the dip angle, ϕ_i is the azimuthal angle, and R_i is the radial distance. Then knowing the location $x_{s,1}$ allows us to recover the dip angle of location $x_{s,2}$, because

$$\theta_2 = \theta_1. \quad (15)$$

Its radial distance from the receiver is given by

$$R_2 = R_1 + V_P \tau_{x_{s,1}, x_{s,2}}(z_{\text{rec}}). \quad (16)$$

In this simple example, these are the two recoverable coordinates from a vertical receiver array using interferometry.

Figure 4 illustrates how event localization using a neighboring fracture works when the known fracture is planar. Any event $x_{s,1}$ lying at the intersection of fracture \mathcal{F}_1 with the cone $\{\theta = \theta_2\}$ will produce a stationary point at the same stationary receiver depth z_{rec} . The stationary lags, $\tau_{x_{s,1}, x_{s,2}}(z_{\text{rec}})$, will vary depending on $x_{s,1}$. Equation 16, however, always holds true.

We observe that the traveltime from any source location to the vertical receiver array does not depend on the azimuth of the source. One therefore cannot obtain constraints on the azimuth beyond those already provided by classical methods through polarization analysis.

Because the total number of sources in fracture \mathcal{F}_1 is typically large, we can expect to have many redundant measurements of the dip angle and radial distance of $x_{s,2}$. We can use these to boost the

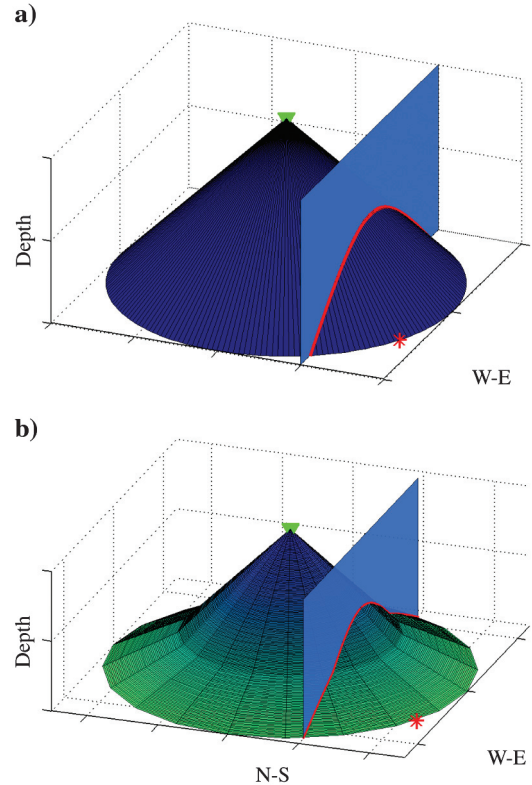


Figure 4. For (a) homogeneous or (b) layered medium, the unknown dip angle (or horizontal offset) and distance along the ray of a source (red star) can be estimated with the help of many stationary sources in the neighboring fracture (vertical plane). Any source along the red curve provides an independent measurement of the distance and horizontal offset of an unknown microseism.

S/N to obtain more precise estimates by appropriate averaging. We present an uncertainty analysis validating this point in the next section.

UNCERTAINTY ANALYSIS

In this section, we quantify microseismic event localization uncertainty for the classical and interferometric methods so that these uncertainties may be compared. We perform the analysis for the case of a homogeneous medium. The approach may be easily generalized to the layered case. Extending it to more general models is a challenge. However, our basic conclusions about the reduction of uncertainty as a result of averaging over a large number of reference events should hold well beyond those two cases. We fix a receiver and then look at estimates of the radial distance and dip from the receiver to the source. Because our method does not offer any estimate of azimuth, its uncertainty remains unexamined, but may be obtained by classical methods.

Classical method

The classical localization method relies on estimates of the traveltime from the event and the polarization of the incoming P- or S-wave. When the recorded signal is noisy, the traveltime and the dip angle of the polarization vector are recovered with some errors (Figure 5):

$$t_p = t_0 \pm \Delta t, \quad \theta = \theta_0 \pm \Delta \theta. \quad (17)$$

The exact distribution of random variables t and θ is dependent on the nature of the noise. However, in the following analysis the

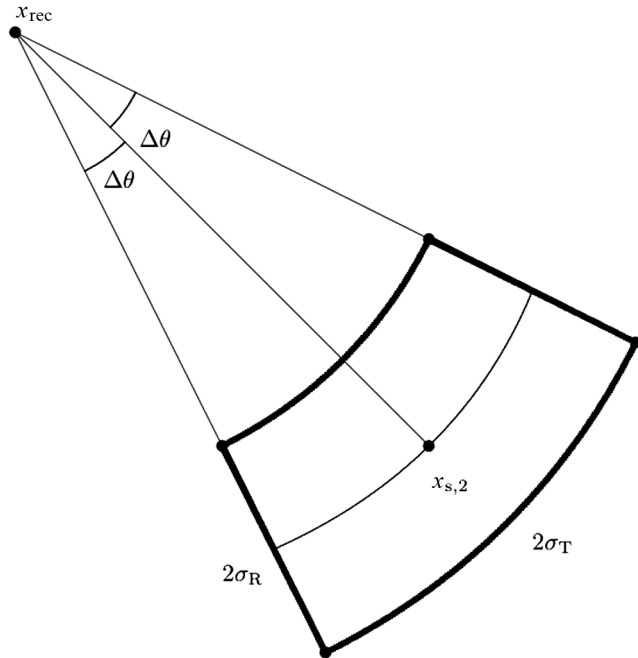


Figure 5. A schematic of the uncertainty variables in the recovered source location for the classical algorithm. The uncertainty in range σ_R is controlled by the error in time picking, while the uncertainty in the transverse direction σ_T is controlled by the error in the estimate of the polarization angle.

perturbations Δt and $\Delta \theta$ may be simply thought of as standard deviations of the error in estimated parameters.

It is convenient to split the uncertainty in event location into two orthogonal directions: along the line of sight (range) and vertically perpendicular to that (transverse or cross-range). The uncertainty in range is determined by the error in picked traveltime and by the assumed velocity

$$\sigma_R = V_p \Delta t.$$

The cross-range (transverse) uncertainty is proportional to the distance from the receiver to the true location of the event; it also depends on the uncertainty in the dip angle:

$$\sigma_T = \|x_{\text{rec}} - x_{s,2}\| \tan \Delta \theta.$$

If the dip uncertainty is sufficiently small, then $\tan \Delta \theta \approx \Delta \theta$, and

$$\sigma_T \approx \|x_{\text{rec}} - x_{s,2}\| \Delta \theta.$$

Stacking these uncertainties over N_{rec} receivers gives

$$\sigma_R^{N_{\text{rec}}} \approx \frac{V_p \Delta t}{\sqrt{N_{\text{rec}}}}, \quad \sigma_T^{N_{\text{rec}}} \approx \frac{d(\mathcal{W}, x_{s,2}) \Delta \theta}{\sqrt{N_{\text{rec}}}}, \quad (18)$$

where $d(\mathcal{W}, x_{s,2})$ is the average radial distance between the monitoring well receivers and the event in the second fracture.

Interferometry

In the proposed method, we construct a correlogram of two common event gathers corresponding to the two event locations $x_{s,1}$ and $x_{s,2}$. The output of the stationary phase analysis of this correlogram is two quantities: the stationary receiver depth z_{rec} and the stationary lag τ . This presumes that all event pairs that do not produce a stationary point have been removed from consideration in a preprocessing step. Because the correlogram is insensitive to the azimuth of seismic events, we can assume without loss of generality in the following analysis that all events have zero azimuth, reducing the problem to two dimensions.

In a noisy environment, the picked stationary receiver depth is a perturbation of the true depth:

$$z_{\text{rec}} = z_{\text{rec}}^0 \pm \Delta z,$$

where z_{rec}^0 is the true stationary receiver depth, and Δz is the error. Note that although receivers are located at discrete depths, the correlogram curve $\tau(z_{\text{rec}})$ can be smoothly interpolated between actual receiver locations to improve depth resolution. Similarly, the stationary lag is also picked with some error:

$$\tau = \tau_0 \pm \Delta \tau.$$

A smooth least-squares interpolation of $\tau(z)$ is expected to further reduce $\Delta \tau$.

Because the location $x_{s,1}$ is known, it is convenient to represent uncertainty in $x_{s,2}$ relative to it (see Figure 6). The range uncertainty σ_R around the true distance $\|x_{s,1} - x_{s,2}\|$ is determined by the error in lag picking and the assumed velocity:

$$\sigma_R = V_p \Delta \tau.$$

The cross-range (transverse) uncertainty is principally determined by the uncertainty in dip angle of $x_{s,2}$ relative to $x_{s,1}$:

$$\sigma_T = \frac{1}{2} \|x_{s,1} - x_{s,2}\| (\tan \Delta \theta^+ + \tan \Delta \theta^-),$$

where $\theta^0 + \Delta \theta^+$ and $\theta^0 - \Delta \theta^-$ are the dip angles of $x_{s,1}$ relative to receiver depths $z_{\text{rec}}^0 - \Delta z$ and $z_{\text{rec}}^0 + \Delta z$, respectively, (see Figure 6)

$$\tan(\theta^0 + \Delta \theta^+) = \frac{z_{s,1} - z_{\text{rec}}^0 + \Delta z}{x_{s,1}},$$

$$\tan(\theta^0 - \Delta \theta^-) = \frac{z_{s,1} - z_{\text{rec}}^0 - \Delta z}{x_{s,1}}.$$

Assuming small errors in the stationary depth pick, namely, $\Delta z \ll x_{s,1}$, and using the Taylor expansion $\arctan(x + \Delta x) \approx \arctan x + (\Delta x / (1 + x^2))$, $\Delta x \ll 1$, we obtain

$$\begin{aligned} \theta^0 + \Delta \theta^+ &= \arctan \left(\frac{z_{s,1} - z_{\text{rec}}^0}{x_{s,1}} + \frac{\Delta z}{x_{s,1}} \right) \\ &\approx \theta^0 + \frac{\Delta z / x_{s,1}}{1 + \left(\frac{z_{s,1} - z_{\text{rec}}^0}{x_{s,1}} \right)^2}. \end{aligned}$$

Hence,

$$\Delta \theta^+ \approx \frac{x_{s,1} \Delta z}{x_{s,1}^2 + (z_{s,1} - z_{\text{rec}}^0)^2}.$$

Likewise, $\Delta \theta^- = \Delta \theta^+$. Applying the small error approximation $\tan x \approx x$, valid for $x \ll 1$, we find that

$$\sigma_T \approx \frac{x_{s,1} \|x_{s,1} - x_{s,2}\| \Delta z}{\|x_{s,1} - x_{\text{rec}}\|^2} = \frac{\cos \theta_0 \|x_{s,1} - x_{s,2}\| \Delta z}{\|x_{s,1} - x_{\text{rec}}\|}.$$

Stacking over all N_s events in the first fracture yields

$$\sigma_R^{N_s} \approx \frac{V_p \Delta \tau}{\sqrt{N_s}}, \quad \sigma_T^{N_s} \approx \frac{\cos \theta_0 d(\mathcal{F}_1, x_{s,2}) \Delta z}{\sqrt{N_s} d(\mathcal{W}, \mathcal{F}_1)}. \quad (19)$$

Here, $d(\mathcal{F}_1, x_{s,2})$ is the average distance between $x_{s,2}$ and events in \mathcal{F}_1 , and $d(\mathcal{W}, \mathcal{F}_1)$ is the average distance from the receivers to the events in \mathcal{F}_1 .

Uncertainty in the reference fracture

We have so far assumed that events in the reference fracture have been located precisely. A more realistic assumption is that, although events that are closer to the monitoring well are resolved better than those that are further away, there remains some uncertainty.

If the range of each event location $x_{s,1}$ has been estimated with some error $\sigma_R^{N_{\text{rec}}}(x_{s,1})$, then that error will propagate to the estimate of $x_{s,2}$. The resulting range uncertainty follows directly from statistical independence of $\Delta \tau$ and $\sigma_R^{N_{\text{rec}}}(x_{s,1})$:

$$(\sigma_R^{N_s}(x_{s,2}))^2 \approx \frac{(\sigma_R^{N_{\text{rec}}}(x_{s,1}))^2 + V_p^2 (\Delta \tau)^2}{N_s}. \quad (20)$$

The uncertainty in the transverse direction as a function of the localization errors in the reference fractures and of the errors in estimating the stationary lag can be derived geometrically as was done for the range error and is illustrated in Figure 7. It is given by

$$\begin{aligned} (\sigma_T^{N_s}(x_{s,2}))^2 &\approx \frac{1}{N_s} \left[\left(1 + \frac{d(\mathcal{F}_1, x_{s,2})}{d(\mathcal{W}, \mathcal{F}_1)} \right)^2 (\sigma_T^{N_{\text{rec}}}(x_{s,1}))^2 \right. \\ &\quad \left. + \frac{\cos^2 \theta_0 d^2(\mathcal{F}_1, x_{s,2})}{d^2(\mathcal{W}, \mathcal{F}_1)} (\Delta z)^2 \right]. \end{aligned} \quad (21)$$

Understanding uncertainty

Here, we give a heuristic interpretation of the uncertainty analysis developed in the previous subsections. We first observe that the number of microseismic events associated with a typical fracture is expected to be much larger than the number of receivers in the monitoring well, i.e., $N_s \gg N_{\text{rec}}$. With this assumption, a comparison of equation 18 to equation 19 reveals that the uncertainty in the location obtained with the interferometric method is expected to be smaller than that obtained with the classical method.

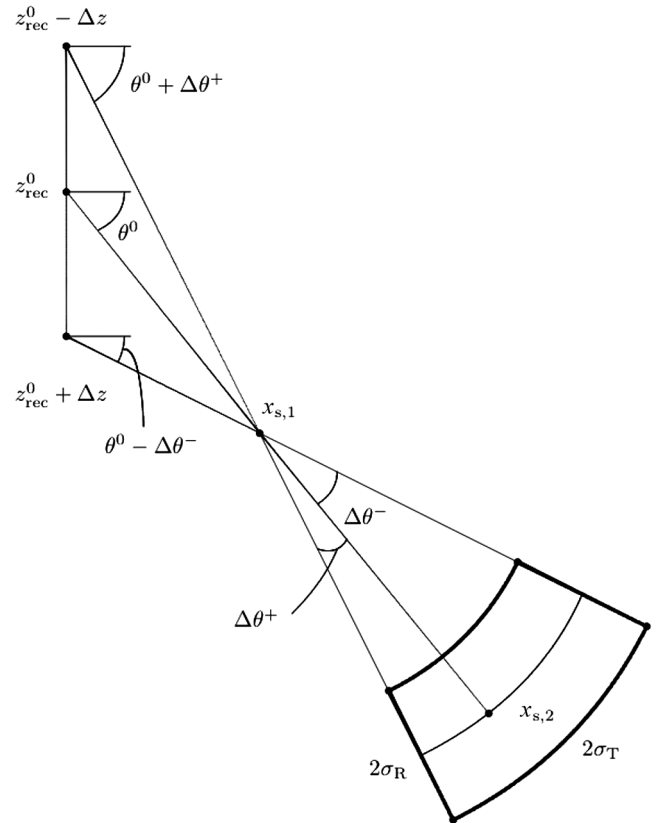


Figure 6. A schematic of the uncertainty variables in the recovered source location for the interferometric algorithm. The uncertainty in range σ_R is controlled by the error in picking the stationary lag in the correlogram, while the uncertainty in the transverse direction σ_T is controlled by radial distance between the two fractures and the error in picking the stationary depth.

The range uncertainty of the interferometric method depends on the error in picking the stationary lag in the correlogram. If the source mechanisms of different events are similar, we can expect very reliable picking in the correlogram. Also, certain types of noise, including additive white noise, are well suppressed by cross-correlation, which makes the proposed method even more robust. On the other hand, the combination of heterogeneous velocity, measurement errors, and differences in source mechanisms are likely to increase the error in recovered locations, both with this method and with classical approaches.

The cross range uncertainty is proportional to the error in picking the stationary receiver depth. For a small number of instruments, this error can be reduced by using interpolation of the correlogram lag times between the recorded depths.

Finally, uncertainty in the velocity model is another factor that will affect the performance of our algorithm. Although we do not address this issue in any detail, we note that the quality of the velocity model is an important factor for the classical method as well. Furthermore, velocity uncertainty between the receiver array and the reference fracture will be largely mitigated with the interferometric method because events in both fractures share much of the path from the first fracture to the observation well.

NUMERICAL RESULTS

In this section, we illustrate the performance of the proposed algorithm with a synthetic experiment. We compare the accuracy of the localization by the classical localization algorithm to the improved interferometric one.

The monitoring well is placed vertically at $(x_{\text{rec}}, y_{\text{rec}}) = (0, 0)$ m. Twenty-three-component receivers are placed in the well equidistantly at depths from 2150 to 2450 m (Figure 8a). The model consists of three layers with interfaces at depths 2200 and 2380 m (Figure 8b). The respective velocities are 3500, 3600, and

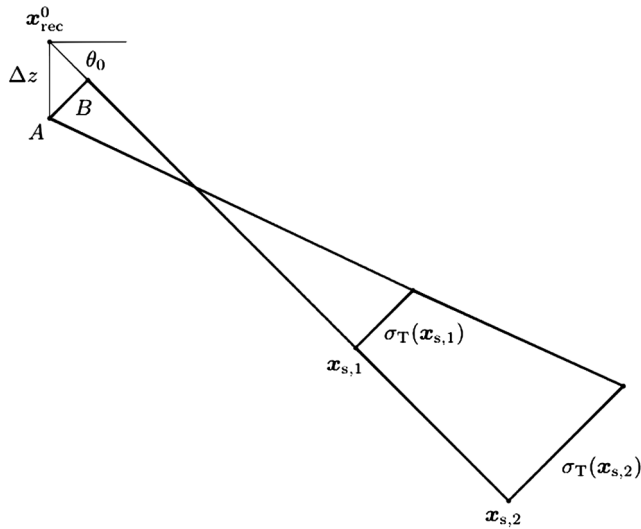


Figure 7. A schematic of the uncertainty variables in the transverse direction in the presence of uncertainty in the reference fracture. Knowing the uncertainty in the stationary receiver location Δz and in the location of the reference event, $\sigma_T(x_{s,1})$, allows the uncertainty in the unknown location, $\sigma_T(x_{s,2})$, to be computed through a simple geometric calculation. Only one-sided deviations from the true locations x_{rec}^0 and $x_{s,1}$ are shown.

3700 m/s. Two vertical planar fractures are positioned next to a monitoring well at a depth of 2300 m. The reference fracture is positioned 100 m away from the well, and the second fracture is 200 m away. Both fractures are 300 meters wide and 100 meters tall. Microseisms are simulated by placing 625 sources on a rectangular grid inside the reference fracture (25 in each direction). All source locations in the first fracture are assumed to be known exactly.

For illustration purposes, we put just a single source in the second fracture at $x_{s,2} = (200, 0, 2300)$ m. The source is a Ricker wavelet (the first derivative of a Gaussian) with a central frequency of 50 Hz. The seismograms are computed using the discrete wavenumber method (Bouchon, 1981) and the reflectivity method (Muller, 1985), and are then contaminated with additive, uncorrelated, Gaussian noise. The S/N, defined as the ratio of the peak amplitude to the standard deviation of the noise, is approximately three in our experiment. An example of a seismogram with and without additive noise is illustrated in Figure 9.

Localization of the event at $x_{s,2}$ is attempted based on the noisy seismogram using the classical and the proposed method. The workflow is as follows. We generate 200 independent realizations of noisy seismograms. For each noisy realization, we localize the source using the classical approach (equation 2) and plot it as a blue dot in Figure 10. Because the proposed method is unable to improve the estimate of the azimuth, we present results in the horizontal offset-depth domain. The blue dots form a cloud centered around

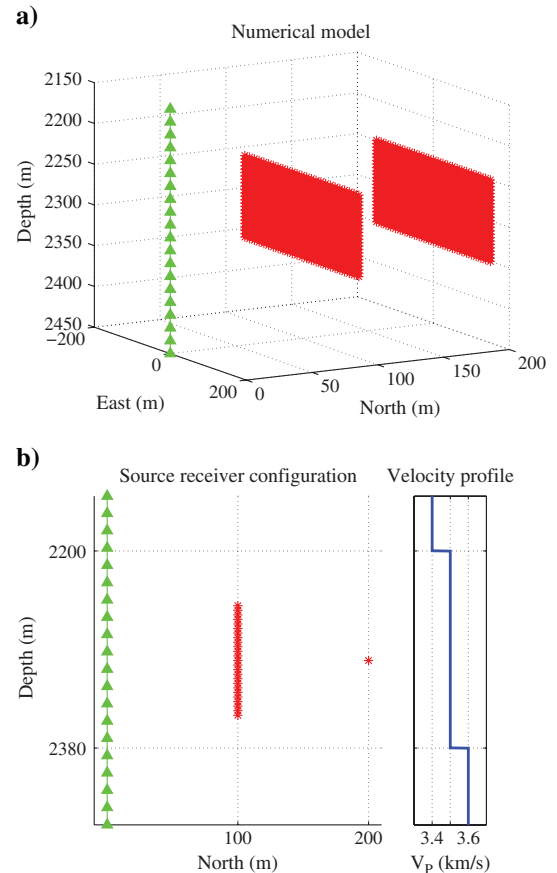


Figure 8. The numerical model contains a monitoring well with two vertical fractures nearby. A source in the more distant fracture is localized using 625 microseismic sources in the nearer fracture.

the true location of the source. The standard deviation of the error in estimated offset of the standard method in this case is approximately 4.5 m. The standard deviation of the depth error is approximately 3.36 m.

We locate the same source with the same geometry using the interferometric method presented here and the microseism locations in the reference fracture. According to the theory, for all events $x_{s,1}$ in the reference fracture, we correlate their seismograms with those of the unknown microseism, and we find the stationary condition of the event in the correlogram, which consists of a stationary receiver and a stationary lag.

A ray is traced from the stationary receiver through the event $x_{s,1}$, and the location $x_{s,2}$ is measured on it using the stationary lag as the traveltimes between the two points. The location of $x_{s,2}$ can be estimated in a layered medium only up to an unknown azimuth. However, both the horizontal offset and the depth are recovered. We show the offset and depth of $x_{s,2}$ so obtained as green stars in Figure 10.

Plotting the interferometric estimates shows a big improvement over the traditional method. The cloud is distributed much closer the true values. The standard deviation of the error in estimated offset of the interferometric method is 0.52 m, and the standard deviation of the depth error is 0.94 m. Therefore, the improvement in localizing

the source is about a factor of 3.6 in depth and nine in offset. Although specific results of this experiment may not translate to other experimental configurations, the superior performance of the interferometric method in this configuration is evident.

CONCLUSIONS

Microseism event localization remains an important and challenging problem. Classical algorithms tend to locate events individually without fully exploiting the coupling and redundancy that exists in the recorded data for multiple fractures. In this paper, we consider a problem with two fractures and a monitoring well. This prototype is typical in hydrofracture monitoring applications in which multiple fractures are sequentially created to improve fluid production. When some fractures are known better than others, we propose to use interferometry to image the less well-located fractures relative to those with more accurate locations. We derive our methodology in the context of general velocity heterogeneity and arbitrary well trajectory, and demonstrate its effectiveness on a layered model with a vertical well. Although we present the uncertainty analysis for a homogeneous medium, the method itself is general and can be expected to offer considerable improvement of event localization in much broader contexts. Applying classical interferometry in a 3D medium requires a 2D array of receivers. When the available data are 1D, basic concepts, such as the stationary phase point, are not uniquely defined, and consequently, standard techniques are not applicable. We have shown that for a vertical array of receivers, although the azimuth information is not improved, estimates of both dip angle and distance can be significantly improved using interferometric techniques. Errors present in the data as well as introduced during the crosscorrelogram analysis lead to localization uncertainty. Each event in the reference fracture, however, acts as an independent measurement. We have shown how to use this redundancy to boost the S/N and thus improve the localization.

ACKNOWLEDGMENTS

The authors would like to thank the ERL Founding Members Consortium, Schlumberger-Doll Research and particularly Stéphane Rondenay for their support of this work. We also thank Jyoti Behura of BP America Inc. and anonymous reviewers for helping us improve this manuscript.

REFERENCES

- Bakulin, A., and R. Calvert, 2004, Virtual source: New method for imaging and 4D below complex overburden: 74th Annual International Meeting, SEG, Expanded Abstracts, 2477–2480.
- Bennett, L., J. L. Calvez, D. R. Sarver, K. Tanner, W. S. Birk, G. Waters, J. Drew, G. Michaud, P. Primiero, L. Eisner, R. Jones, D. Leslie, M. J. Williams, J. Govenlock, R. C. R. Klem, and K. Tezuka, 2005, The source for hydraulic fracture characterization: *Oilfield Review/Schlumberger*, **17**, 42–57.
- Borcea, L., G. Papanicolaou, and C. Tsogka, 2005, Interferometric array imaging in clutter: *Inverse Problems*, **21**, 1419–1460, doi: [10.1088/0266-5611/21/4/015](https://doi.org/10.1088/0266-5611/21/4/015).
- Bouchon, M., 1981, A simple method to calculate Green's functions for elastic layered media: *Bulletin of the Seismological Society of America*, **71**, 959–971.
- Curtis, A., H. Nicolson, D. Halliday, J. Trampert, and B. Baptie, 2009, Virtual seismometers in the subsurface of the earth from seismic interferometry: *Nature Geoscience*, **2**, 700–704, doi: [10.1038/ngeo615](https://doi.org/10.1038/ngeo615).
- de Franco, R., and G. Musacchio, 2001, Polarization filter with singular value decomposition: *Geophysics*, **66**, 932–938, doi: [10.1190/1.1444983](https://doi.org/10.1190/1.1444983).
- Derode, A., E. Larose, M. Campillo, and M. Fink, 2003, How to estimate the Green's function of a heterogeneous medium between two passive

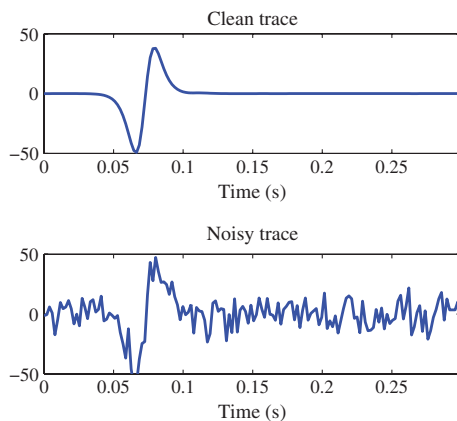


Figure 9. An example of a clean seismogram and of the same seismogram with additive uncorrelated noise superimposed on it.

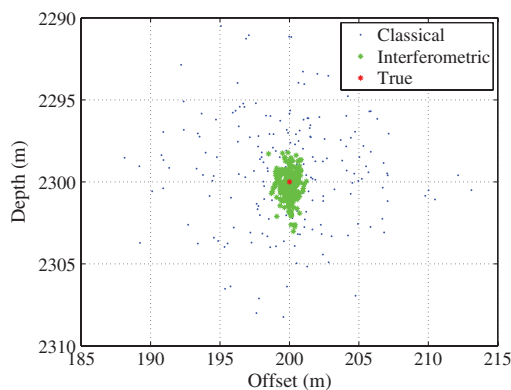


Figure 10. Localization results plotted in the offset-depth domain. The new method offers significantly improved estimates.

- sensors? Application to acoustic waves: *Applied Physics Letters*, **83**, 3054–3056, doi: [10.1063/1.1617373](https://doi.org/10.1063/1.1617373).
- Djikpesse, H., S. Dong, J. Haldorsen, and D. Miller, 2009, Comparing interferometric migration and mirror imaging of 3D VSP free-surface multiples: Noise and Diffuse Wavefields: *DGG-Mitteilungen*, 79–86.
- House, L., 1987, Locating microearthquakes induced by hydraulic fracturing in crystalline rock: *Geophysical Research Letters*, **14**, 919–921, doi: [10.1029/GL014i009p00919](https://doi.org/10.1029/GL014i009p00919).
- Huang, Y. A., J. Chen, and J. Benesty, 2006, Time delay estimation and acoustic source localization, in *acoustic MIMO signal processing*, Signals and communication technology: Springer, 215–259.
- Lu, R., M. E. Willis, X. Campman, J. Ajo-Franklin, and M. N. Toksöz, 2008, Redatuming through a salt canopy and target oriented salt-flank imaging: *Geophysics*, **73**, S63–S71, doi: [10.1190/1.2890704](https://doi.org/10.1190/1.2890704).
- Michaud, G., D. Leslie, J. Drew, T. Endo, and K. Tezuka, 2004, Microseismic event localization and characterization in a limited aperture HFM experiment: 74th Annual International Meeting, SEG, Expanded Abstracts.
- Müller, G., 1985, The reflectivity method: A tutorial: *Journal of Geophysics*, **58**, 153–174.
- Pearson, C., 1981, The relationship between microseismicity and high pore pressures during hydraulic stimulation experiments in low permeability granitic rocks: *Journal of Geophysical Research*, **86**, 7855–7864, doi: [10.1029/JB086iB09p07855](https://doi.org/10.1029/JB086iB09p07855).
- Rickett, J., and J. Claerbout, 1996, Passive seismic imaging applied to synthetic data: Technical Report 92, Stanford Exploration Project, http://sepwww.stanford.edu/public/docs/sep92/james1/paper_html/, accessed 3 December 2011.
- Schuster, G. T., J. Yu, J. Sheng, and J. Rickett, 2004, Interferometric/daylight seismic imaging: *Geophysical Journal International*, **157**, 838–852, doi: [10.1111/gji.2004.157.issue-2](https://doi.org/10.1111/gji.2004.157.issue-2).
- Schuster, G. T., and M. Zhou, 2006, A theoretical overview of model-based and correlation-based redatuming methods: *Geophysics*, **71**, SI103–SI110, doi: [10.1190/1.2208967](https://doi.org/10.1190/1.2208967).
- Snieder, R., 2004, Extracting the Green's function from the correlation of coda waves: A derivation based on stationary phase: *Physical Review E*, **69**, 046610.1–046610.8, doi: [10.1103/PhysRevE.69.046610](https://doi.org/10.1103/PhysRevE.69.046610).
- Wapenaar, K., 2004, Retrieving the elastodynamic Green's function of an arbitrary inhomogeneous medium by cross correlation: *Physical Review Letters*, **93**, 254301-1–254301-4, doi: [10.1103/PhysRevLett.93.254301](https://doi.org/10.1103/PhysRevLett.93.254301).
- Wapenaar, K., J. T. Fokkema, and R. Snieder, 2005, Retrieving the Green's function in an open system by cross correlation: A comparison of approaches: *Journal of the Acoustical Society of America*, **118**, 2783–2786, doi: [10.1121/1.2046847](https://doi.org/10.1121/1.2046847).
- Zoback, M. D., C. A. Barton, M. Brudy, D. A. Castillo, T. Finkbeiner, B. R. Grollmund, D. B. Moos, P. Peska, C. D. Ward, and D. J. Wiprut, 2003, Determination of stress orientation and magnitude in deep wells: *International Journal of Rock Mechanics and Mining Sciences and Geomechanics Abstracts*, **40**, 1049–1076, doi: [10.1016/j.ijrmmms.2003.07.001](https://doi.org/10.1016/j.ijrmmms.2003.07.001).